Split-Ring Coupled Low-Cost Antenna with Electromagnetic Bandgap (EBG) Superstrates to Produce Tri-Bands and High Gains

Supakit KAWDUNGTA [1], Danai TORRUNGRUENG [2], Hsi-Tseng CHOU [3]

[1] Faculty of Engineering, Rajamangala University of Technology Lanna, Chiang Mai, Thailand
[2] Research Center of Innovation Digital and Electromagnetic Technology, Department of Teacher Training in Electrical Engineering, Faculty of Technical Education, King Mongkut's University of Technology North Bangkok, Bangkok 10800, Thailand
[3] Graduate Institute of Communication Engineering, National Taiwan University, Taipei 10617, Taiwan

supakitting@rmutl.ac.th, dtg@ieee.org, chouht@ntu.edu.tw

Submitted October 8, 2023 / Accepted November 29, 2023 / Online first December 9, 2023

Abstract. *In this paper, a novel tri-band low-cost antenna covering the desired frequencies is presented. The architecture is formed by a printed dipole coupled by a split-ring within an electromagnetic bandgap (EBG) structure for high radiation gains. The printed dipole is placed beneath two dielectric superstrates, and the coupling split-ring is placed on its top. The proposed antenna is excited by the printed dipole with a coaxial connector. It is placed in the middle cavity formed by two dielectric superstrates and a metal reflector as the simple EBG structure. The simulation results show three resonant frequencies at 1.42, 2.39 and 5.40 GHz respectively, with uni-directional radiation patterns and high gains enhanced by the EBG structure. Experimental measurements over an antenna prototype validate the results of reflection coefficients and radiation patterns. It is found that the gains are 8.50, 6.00 and 8.10 dBi at 1.42, 2.39 and 5.00 GHz respectively, which are sufficient for L-band and WiFi applications. In addition, simulation and measurement results are in good agreement.*

Keywords

Electromagnetic bandgap, split-ring, superstrates, tri-band

1. Introduction

Future mobile communications will be formed by three-dimensional (3-D) wireless networks hybridized by ground mobile networks of 4G/5G (4th Generation/5th Generation), non-terrestrial networks (NTN), and satellites. They will be used to form the internet and provide high-speed data transmission. Multi-band antennas simultaneously accommodating these frequency bands are most desired for easy implementation, cost reduction and reliability enhancement due to the fact that the mutual interferences can be adequately treated in advance.

In the past, many multi-band antenna designs have been pursued in wireless applications. In [1], a multi-band antenna was proposed in the configuration of an antenna array that consists of two antenna elements in low and high bands, operating in 690–960 MHz and 1.70–2.70 GHz respectively, for base station applications [1]. However, the structure of the proposed antenna is complicated by using the array technique. The tri-band antenna is introduced for UAV (Unmanned Aerial Vehicle) applications with omni-direction and horizontal polarization. The antenna structure consists of a folded patch inside a metal box with a vertical slot, which can operate in the frequency ranges of 840.50 to 845 MHz, 1430–1444 MHz and 2408–2440 MHz, respectively. However, it provides a low gain around 2–5 dBi [2]. In [3], asymmetrically barbed dipole antennas are introduced as tri-band antennas with circular polarization for GPS (Global Positioning System) applications, where the operating frequency ranges are 1.131 to 1.312 GHz, 1.369–1.421 GHz and 1.543–1.610 GHz. The antenna is in the inverted pyramidal cavity and provides a uni-directional radiation pattern with an antenna gain of around 7–8 dBic. However, its antenna structure is complicated. In [4], a multi-band antenna is formed by integrating a feeding monopole with five slot-loaded microstrips and an SRR (Split Ring Resonator) element to produce five frequency bands. On the other hand, the SRR was also used to form a loaded Koch star fractal antenna with five frequency resonances [5]. These demonstrated that the SRR elements could be loaded to generate multi-resonant frequencies. However, they usually radiate low antenna gains, which will be improved significantly in this paper. As a result, multi-band antennas can be integrated into multi-band systems.

This paper presents a novel tri-band split-ring coupled antenna with a pair of electromagnetic bandgap (EBG)

DOI: 10.13164/re.2024.0024

superstrates to enhance antenna gains for modern wireless communications. This antenna structure consists of a printed dipole placed beneath a dielectric substrate. This printed dipole excites the antenna radiation through a coupling split-ring placed on the top of a dielectric substrate. The split-ring coupled antenna is placed in the middle cavity formed by two dielectric superstrates and a metal reflector as the simple EBG structure for gain enhancement. The proposed antenna can achieve three operational frequency bands at 1.38, 2.45 and 5.50 GHz with high radiation gains (6–8 dBi) and uni-directional radiation patterns.

The novelty of this work can be summarized as follows. The creation of the tri-bands employs electromagnetically coupling mechanisms of parasitic elements, where both split rings and EBG structure serve as the external parasitic elements for multi-band creation. The simple low-cost EBG structure assists in producing an additional low-frequency L-band resonance and enhancing the radiation gain at high frequencies. The resulting beamwidths are shown to be broad by 70–90 degrees at low frequencies and narrow by 20 degrees at high frequencies. Note that traditional designs require large antenna structures and have difficulty enhancing gains by forming antenna arrays.

The rest of this paper is organized as follows. Section 2 presents the proposed antenna structure. Parametric studies and full-wave simulation results are illustrated in Sec. 3. In addition, Section 4 provides measurement results. Finally, conclusions are given in Sec. 5.

2. Antenna Structure

2.1 Antenna Architecture

The proposed structure of the tri-band split-ring coupled antenna embedded in the simple low-cost EBG structure is illustrated in Fig. 1, where its structure consists of two FR4 dielectric superstrates (1.60 mm in thickness) and a metal reflector. The antenna's main body is implemented on an FR4 dielectric substrate ($\varepsilon_r = 4.30$, tan $\delta = 0.02$ and thickness of 1.60 mm) inside the EBG structure, where ε_r is its dielectric constant and tan δ is its loss tangent. On the top surface of the FR4 substrate, a double SRR [6], [7] is implemented by two concentric microstrip rings, as shown in Fig. 1(a), where the open sections of the inner and outer rings face to the opposite directions. They may form two resonances in conjunction with the essential dipole feeding implemented on the bottom face of the FR4 substrate, as shown in Fig. 1(b). The formation of the antenna body with the EBG structure is demonstrated in Fig. 1(c).

Note that, the EBG structure has two rectangular dielectric superstrates on the top and a ground plane below the proposed antenna. The actual feeding is a coaxial feed at the bottom of this FR4 substrate to excite the dipole feeding structure. These feeding and radiating structures are

Antenna Parameter	Description	Size (mm)
D	The diameter of the split-ring antenna	124
d	The diameter of a small split-ring antenna	88
g_1	The gap of the split-ring antenna	16
g_2	The gap of a small split-ring antenna	20
t_1	The thickness of the split-ring antenna	6
t_2	The thickness of a small split-ring antenna	5
dl	The length of the dipole	33
t_d	The thickness of the dipole	4
g_3	The gap of the dipole	4
G_1	The distance between the dielectric superstrate and the reflector	62
G_2	The distance between two dielectric superstrates	53
W	The total width of the dielectric substrate and reflector	180
L	The total length of the dielectric substrate and reflector	180

Tab. 1. Geometric parameters of split-ring coupled antenna with EBG.

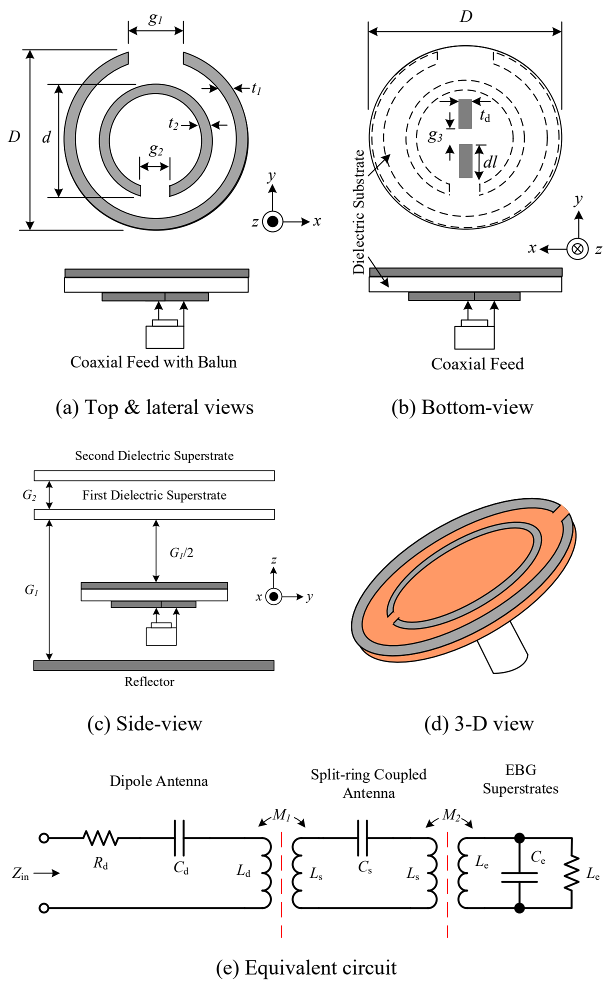

Fig. 1. The structure of the tri-band split-ring coupled antenna within the EBG structure.

placed in the air cavity formed by the EBG structure, as shown in Fig. 1(c), where the separation distances are labeled. They were achieved by parametric fine-tuning. The three EBG plates are rectangular with a side of 180 mm. The prospective 3-D view in Fig. 1(d) shows the resulting antenna architecture for easy understanding. Detailed geometric parameters are labeled in Fig. 1 and summarized in Tab. 1. The values listed are the final designed parameters obtained from the optimized full-wave simulations for experimental measurement validation. Additionally, Figure 1(e) illustrates the equivalent circuit of the proposed antenna. In [8], the authors proposed the synthesis of the equivalent circuit of each type of split-ring coupled antenna. The proposed antenna can be divided into three main components; i.e., dipole antenna, split-ring coupled antenna, and EBG superstrates. The equivalent circuit of the dipole antenna consists of a series *RLC* circuit (L_d, C_d, and R_d), where that of the split-ring coupled antenna comprises an *LC* resonator circuit (L_s and C_s), with a coupling coefficient of M_1. Note that the equivalent circuit of the EBG superstrate includes a parallel *RLC* circuit (L_e, C_e, and R_e) with a coupling coefficient of M_2.

2.2 Operational Mechanism

The operational mechanisms of this tri-band antenna are interpreted in the following discussion. In this design, the SRR element is the major element for the multiple frequency resonances. Note that SRR elements were initially introduced as the forming elements in [6] to realize a Mu negative (MNG: μ-negative) material or a left-handed (LH) material. They are generally referred to as artificial materials or metamaterials. The nonconventional natures of the SRR material make it suitable to serve as an effective parasitic element on the top of the feeding dipole, as shown in Fig. 1, to produce multiple resonances. This integration can have three frequency resonances, as pointed out in [4], [5]. In [4], a multi-band antenna is formed by integrating a feeding monopole with five slot-loaded microstrips and an SRR element to produce five frequency bands. On the other hand, the SRR was also used to form a loaded Koch star fractal antenna with five frequency resonances [5]. These demonstrated that the SRR elements could be loaded to generate multi-resonance frequencies. However, they radiate low antenna gains, which will be improved in this paper.

The gain enhancement is performed by incorporating the SRR-loaded dipole antenna within the EBG structure. The two EBG dielectric superstrates, separated by a distance of G_2, are placed on the top of the antenna with a separation distance of $G_1/2$. The metal reflector is put below the antenna at a distance of G_1 away from the first dielectric superstrate, as shown in Fig. 1(c). The EBG superstrates form a resonant cavity to enable the antenna to radiate uni-directional patterns and improve the antenna gain. The superstrate structures have been used to improve the antenna gain and bandwidth, as found in [9], [10], [11]. The criteria for using EBG superstrates have been discussed in detail in [12], [13]. The EBG structures of lossless periodic multilayers were analytically studied by a conjugate characteristic-impedance transmission line (CCITL) model. The study shows that a proper number of unit cells of EBG structures can provide better directivity [12].

3. Parametric Studies and Full-Wave Simulation Results

Parametric studies were performed using CST Microwave Studio [14] to exhibit basic behaviors of the tri-band split-ring coupled antenna embedded in the EBG

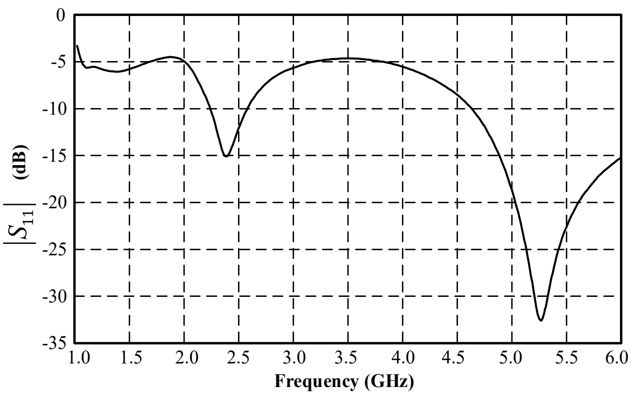

Fig. 2. Simulated $|S_{11}|$ of the split-ring coupled antenna with a dipole feed.

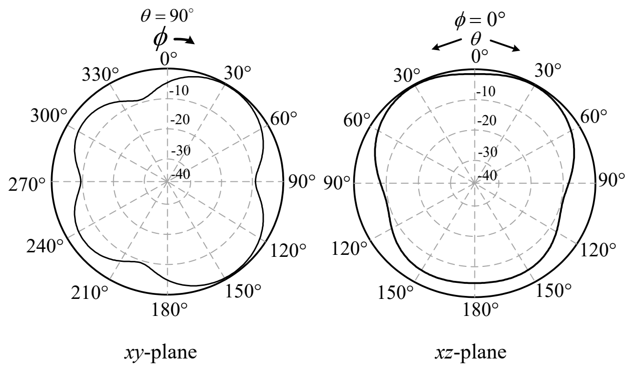

(a) at 2.45 GHz

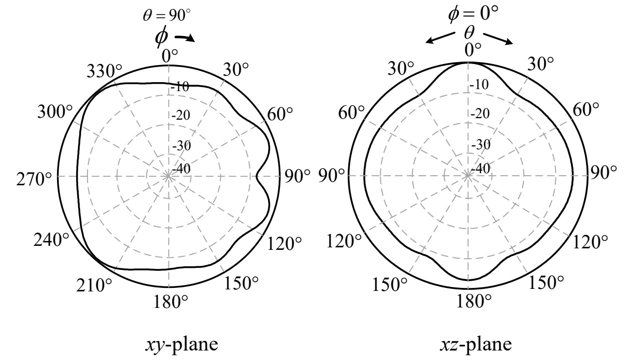

(b) at 5.25 GHz

Fig. 3. Simulated radiation patterns of the split-ring coupled antenna with a dipole feed at 2.45 GHz and 5.25 GHz without incorporating the EBG superstrates.

structure. Note that the SRR on the FR4 dielectric substrate coupling with the dipole feed is the major radiator of the proposed antenna. Their dimensions will influence the essential characteristics of resonances and will be examined thoroughly.

Figure 2 shows the plot of $|S_{11}|$ of the split-ring coupled antenna with the dipole feed versus frequency, where two resonances are shown for the frequency bands of 2.24–2.56 GHz and 4.60–6.00 GHz, respectively. The radiation patterns at 2.45 GHz and 5.25 GHz are shown in Figs. 3(a) and (b) respectively, where uni-directional patterns with small antenna gains of 4.00 dBi and 4.52 dBi are shown.

Next, the split-ring coupled antenna's dipole feed length (*dl*) is increased from 30 to 40 mm for a parametric study. The simulated results of $|S_{11}|$ are shown in Fig. 4, where the length of the dipole directly determines the two resonance frequencies. It is found that the resonant frequencies shift to lower values as the length increases.

Next, one considers the effects of the split-ring's diameter. The inner split-ring's diameter (*d*) is 30 mm, while the outer split-ring antenna diameter (*D*) varies from 110 to 150 mm. The widths of the circular microstrips remain unaltered. The simulated curves of $|S_{11}|$ are shown in Fig. 5 (a), where it is seen that the resonance frequencies remain unchanged except for their levels. This behavior indicates that this parameter changes the input impedance to alter the matching at the resonant frequencies. A tradeoff between high and low-frequency resonances should be considered.

In contrast, the inner ring's diameter (*d*) brings more impact on the resonant frequencies. In the examination, *d* varies from 50 to 90 mm while *D* is set to 150 mm. Figure 5(b) depicts the effects of simulated $|S_{11}|$ on both resonance frequencies. It is seen that a proper value of *d* at 70 mm can produce two resonance frequencies at 1.89 and 4.24 GHz, respectively. These two studies show that a double split-ring coupling to a dipole feed can have two resonant frequencies.

The gaps of the split-rings' two opposite open sections, g_1, and g_2, are examined in Fig. 6(a) and (b), respectively. It is seen that the gap (g_1) of the outer split-ring does

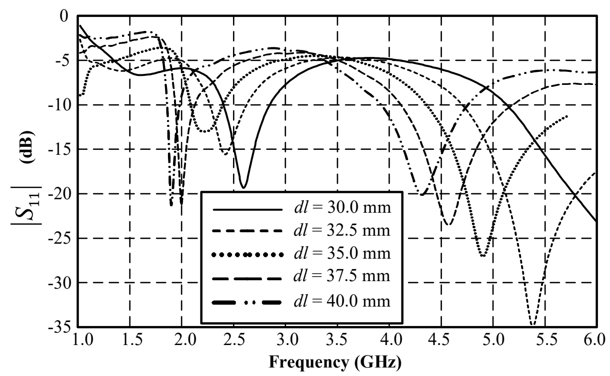

Fig. 4. Simulated $|S_{11}|$ of the split-ring coupled antenna versus dipole feed length (*dl*) for excitation.

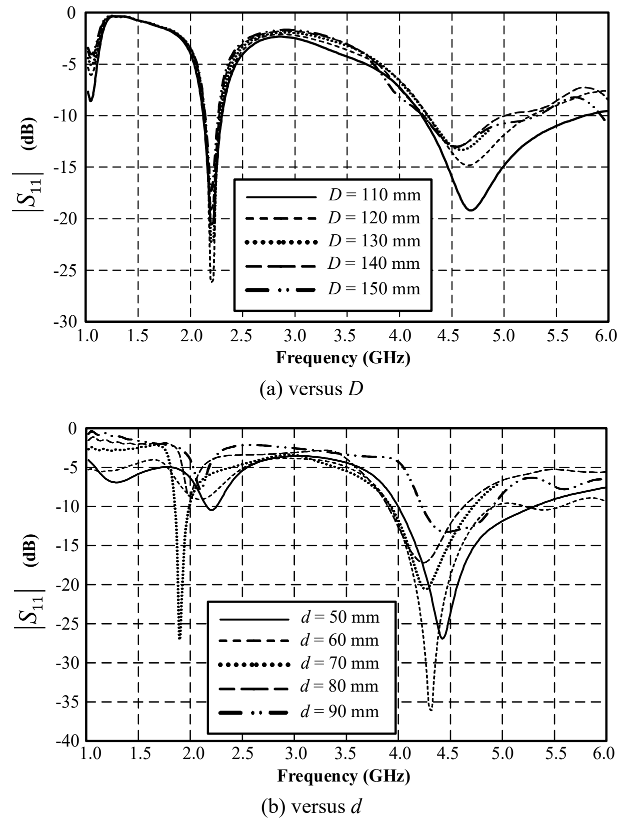

Fig. 5. Simulated $|S_{11}|$ with respect to the outer and inner split-rings' diameters, *D* and *d*, in (a) and (b), respectively.

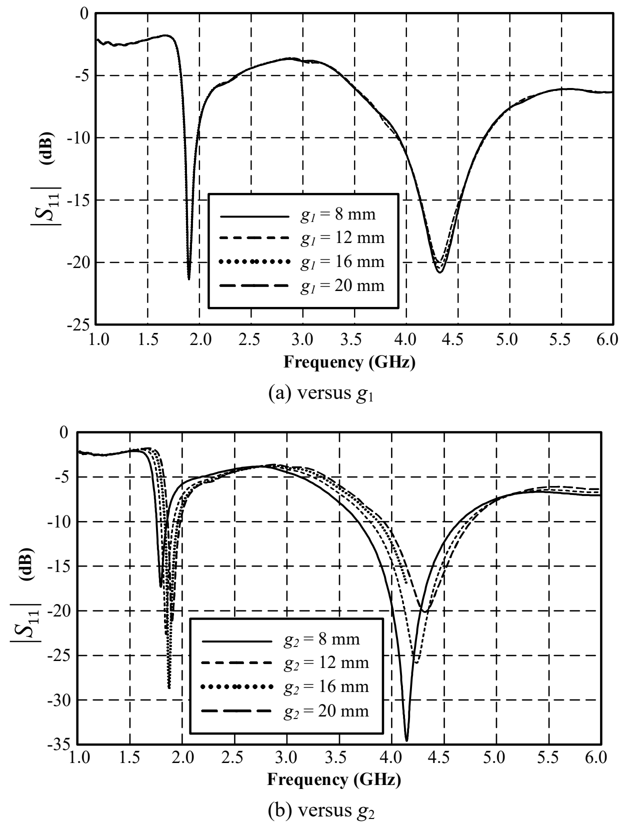

Fig. 6. Simulated $|S_{11}|$ curves with respect to the outer and inner split-rings' open gaps, g_1, and g_2 in (a) and (b), respectively.

not significantly alter the nature of $|S_{11}|$ when it varies from 8 to 20 mm. On the other hand, the gap (g_2) of the inner split-ring has some impact on the resonant frequencies when it varies from 8 to 20 mm. In these cases, a smaller g_2 shifts the resonant frequencies to the lower sides, caused by the influence of impedance matching.

The third resonance is introduced by inserting the split-ring antenna structure into the cavity formed by the EBG superstrates. It is noted that the incorporation of the EBG superstrates will also alter the positions of the first two resonant frequencies due to the interactions between the antenna and the EBG superstrates. The basic properties of antenna radiation embedded in EBG structures have been studied in [12] by placing a Hertzian dipole, as shown in Fig. 7. For the proposed antenna in this paper, the EBG structure consists of four layers ($N = 4$) superstrates in a unit cell, which is terminated by a perfect electric conductor (PEC) ($Z_S = 0\ \Omega$).

Figure 8 shows the dispersion diagram of this EBG structure, estimated by using (8) in [12], for the frequency range from 1 to 8 GHz, where the EBG parameters in Fig. 2 are employed, and the observation angle of antenna radiation is at $\phi = 90°$ and $\theta = 45°$, where ϕ and θ are the azimuth and elevation angles, respectively. The dispersion diagrams are shown in Fig. 8 for both TE (Transverse Electric) and TM (Transverse Magnetic) modes existing in the EBG structure in Fig. 7 [12], which overlap in this case. In Fig. 8, l_U is the total length of each unit cell ($l_U = l_1 + l_2 + l_3 + l_4$) and β_C is the effective propagation constant of the CCITL to model the unit cell. In this study,

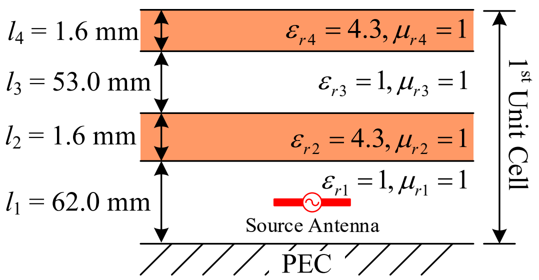

Fig. 7. EBG structure configuration [12].

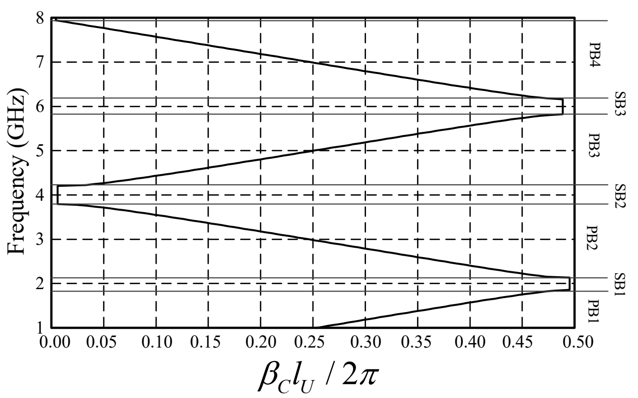

Fig. 8. The dispersion diagram of both TE and TM modes for the given EBG structure at an observation angle of $\phi = 90°$ and $\theta = 45°$.

the operating frequencies of 1.42, 2.39 and 5.00 GHz are in the passbands of PB1, PB2 and PB3 respectively, as expected. Note that PB*i* and SB*i* in Fig. 8 denote the *i*th passband and stopband in the frequency range of interest, respectively.

The coupled split-ring antenna with a dipole feed is sandwiched by the EBG structures at the center, as shown in Fig. 1(c). It is seen that these EBG structures produce a low-frequency resonance while shifting the original two resonances to higher frequencies. As shown in Fig. 5(a) and (b), the resonant frequencies were near 1.89 GHz and 4.24 GHz, now shifting to 2.39 GHz and 5.40 GHz. The resonant frequency produced by the EBG coupling is

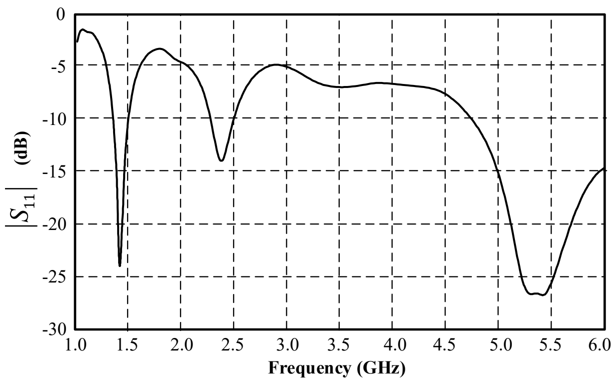

Fig. 9. Simulated $|S_{11}|$ of the split-ring coupled antenna with the dipole feed in the cavity formed by the EBG superstrates.

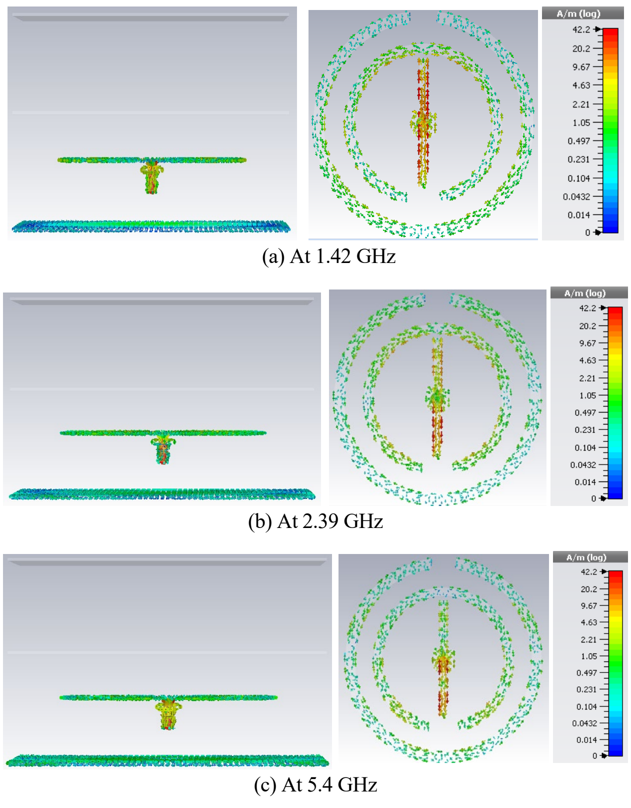

(a) At 1.42 GHz

(b) At 2.39 GHz

(c) At 5.4 GHz

Fig. 10. Simulated current distributions of the split-ring coupled antenna with the dipole feed in the cavity formed by the EBG superstrates.

1.42 GHz. These three resonant frequencies at 1.42, 2.39, and 5.40 GHz are well shown in Fig. 9. To understand the radiation mechanisms of the proposed antenna better, the current distributions are shown in Fig. 10(a)–(c) at these three resonant frequencies. It is seen that the dominant current contributions are on the dipole and are coupled to the SRR structure for multi-band resonances.

The radiation patterns of the fine-tuned antenna incorporating the EBG superstrates are shown in Fig. 11(a)–(c) for 1.42, 2.39, and 5.40 GHz, respectively. It is seen that all three patterns exhibit uni-directional patterns with high antenna gains. They are 8.50, 6.00, and 8.10 dBi at 1.42, 2.39, and 5.40 GHz, respectively. It is noted that the dipole nature results in null fields along the *y*-axis direction, consistent with the dipole's orientation, as shown in Fig. 11(a). The front-back gain ratio is roughly 8.00 dB to make the radiation uni-directional.

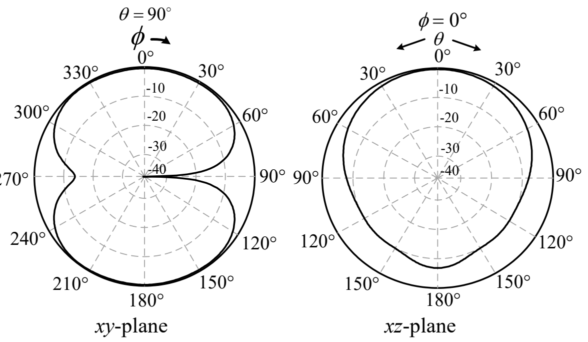

(a) at 1.42 GHz

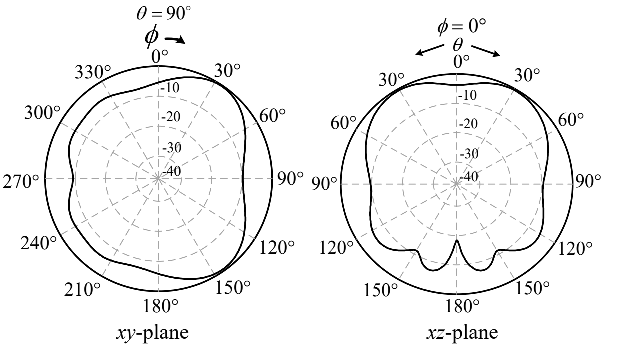

(b) at 2.39 GHz

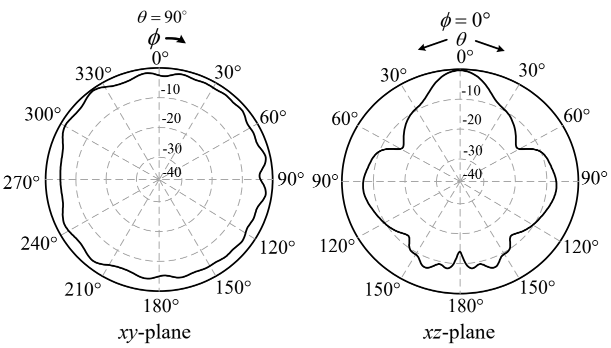

(c) at 5.40 GHz

Fig. 11. Simulated radiation patterns of the split-ring coupled antenna with a dipole feed in the cavity formed by the EBG superstrate at 1.42, 2.39, and 5.40 GHz in (a)–(c), respectively.

Radiation Efficiency (%)			
Freq. (GHz)	1.42	2.39	5.40
Without EBG	95.80	95.50	91.62
With EBG	93.24	93.56	90.16

Tab. 2. Radiation efficiency comparison of the split-ring coupled antenna with and without the EBG structures.

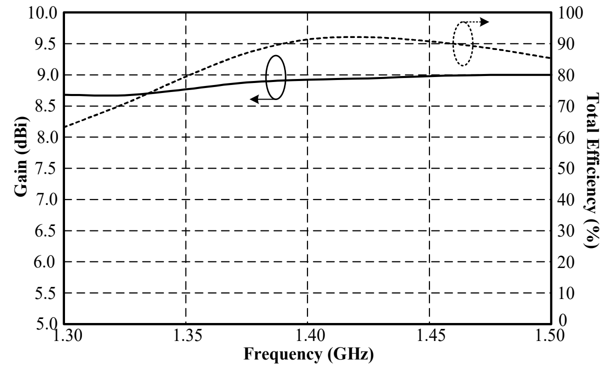

(a) at 1.42 GHz band

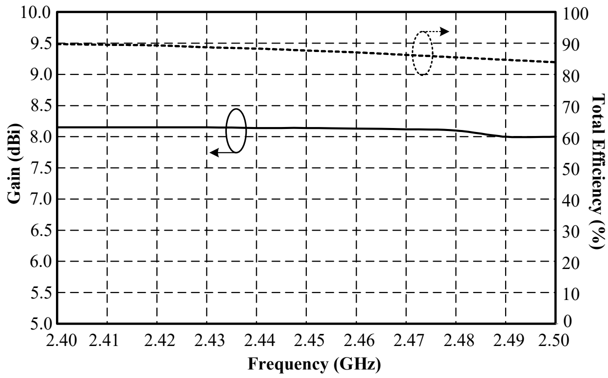

(b) at 2.39 GHz band

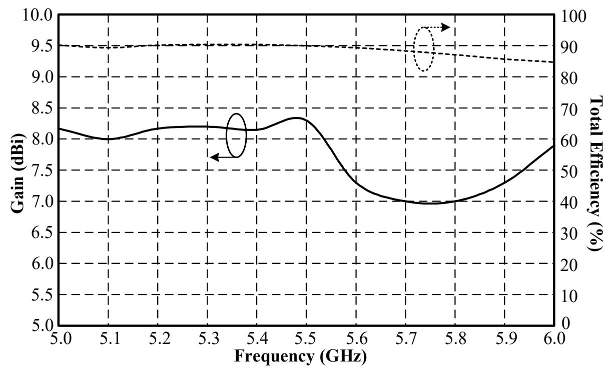

(c) at 5.40 GHz band

Fig. 12. Simulated gain and total efficiency versus frequency of the proposed antenna at 1.42, 2.39, and 5.40 GHz bands in (a)–(c), respectively.

On the other hand, the radiation patterns at the two higher frequency bands in Fig. 11(b) and (c) can be compared to those in Fig. 3(a) and (b) to exhibit the effectiveness of the EBG superstrates in altering the antenna gains and directivities, respectively. First, it is seen that the radiation patterns under the incorporation of EBG superstrates are more directional because of the existence of the ground reflector. On the *x*-*y* plane, the patterns are much smoother with reduced levels of ripples. In terms of gain enhancement, they are increased from 4.00 and 4.52 dBi in Fig. 3(a) and (b) to 6.00 and 8.10 dBi, indicating 2.00 and 3.58 dB improvements for the two frequency bands, respectively.

In addition, the radiation efficiencies of the split-ring coupled antenna with and without the EBG structures are shown in Tab. 2. The radiation efficiencies of the proposed antenna with the EBG are 93.24% at 1.42 GHz, 93.56% at 2.39 GHz, and 96.16% at 5.40 GHz, respectively, which are slightly smaller than those for the case without the EBG, respectively. The proposed antenna architecture's simulated gain and total efficiency versus frequency are shown in Fig. 12(a)–(c) at 1.42, 2.39, and 5.40 GHz bands, respectively. It is seen that the total efficiency is more than 60% in all frequency bands, and the antenna gains are more than 7.00 dBi.

4. Measurement Results

The proposed split-ring coupled antenna with a dipole feed incorporating the EBG structure is fabricated for measurement validation as shown in Fig. 13. The components were manufactured separately and then assembled by hand. In particular, all substrates are integrated using thin plastic pillars with screws to fasten them on the two alternative corners. Note that these pillars may cause some interferences at high frequencies, which are small at the low-frequency band.

The measured $|S_{11}|$ is shown in Fig. 14, where the achieved frequency bands are at 1.32–1.50, 2.10–2.80 and 4.90–5.20 GHz respectively, based on the –10 dB threshold of $|S_{11}|$. These resonant frequencies deviate slightly from the simulation results by about 8%, where the general trend remains the same. Note that there are two resonances nearby to form a broader bandwidth than the simulated one at the 2.40 GHz band. These deviations are attributed to the complete feeding structure and extra plastic pillars supporting the split-ring coupled antenna, which has yet to be incorporated into the simulations. The radiation patterns with co- and cross-polarizations are also measured at three resonant frequencies of 1.42, 2.39 and 5.00 GHz as shown in Fig. 15(a)–(c), respectively. These measurement patterns are compared to those obtained from the simulations to show their consistency. It is found that they are in good agreement. In addition, the measured antenna gains are 8.00, 4.50, and 7.00 dBi at 1.42, 2.39 and 5.00 GHz, respectively. Compared to the simulation results, the gain at 1.42 GHz is consistent. The measurement has roughly 0.50, 1.50, and 1.10 dB losses attributed to the connector and cable losses in the measurement setup at the two higher frequencies. In these cases, the connector loss is nearly 0.80 dB. The plastic pillars may also cause some diffraction destructions. It is found that the resulting antenna

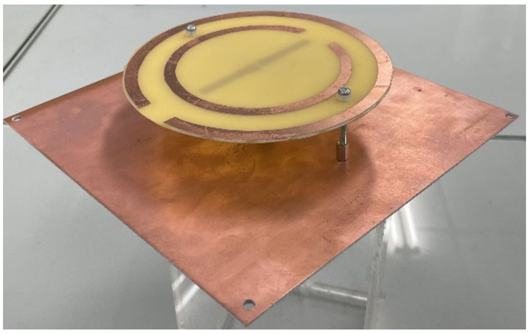

(a) The split-ring coupled antenna with a ground plane

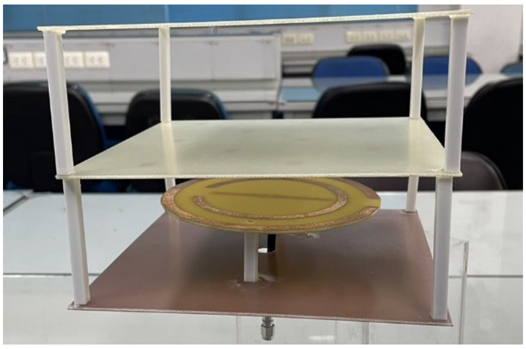

(b) The complete split-ring coupled antenna

Fig. 13. Prototype of the split-ring coupled antenna with a dipole feed in the cavity formed by the EBG superstrates. In (a), the two dielectric substrates are removed to show the split-ring coupled antenna architecture, while (b) shows the complete prototype.

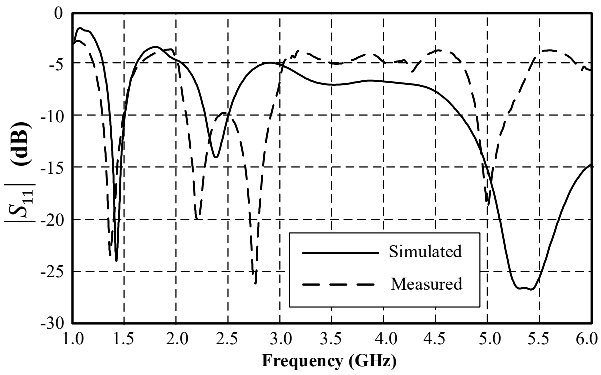

Fig. 14. Measured $|S_{11}|$ patterns of the split-ring coupled antenna with dipole feed in EBG.

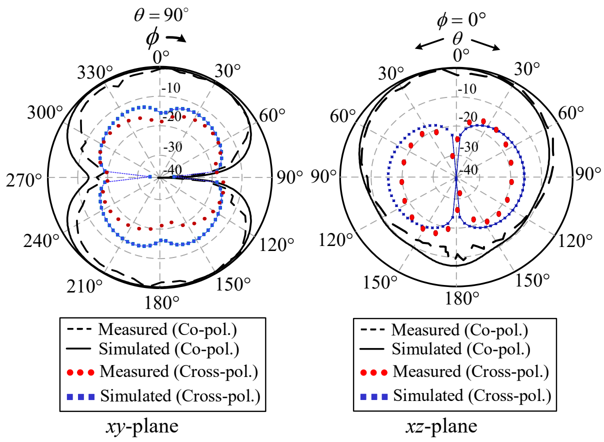

(a) at 1.42 GHz

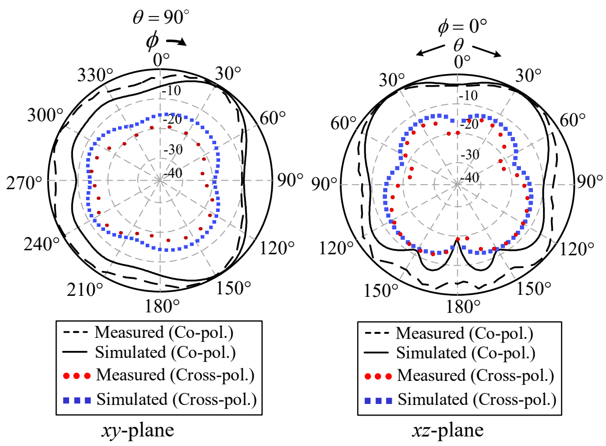

(b) at 2.39 GHz

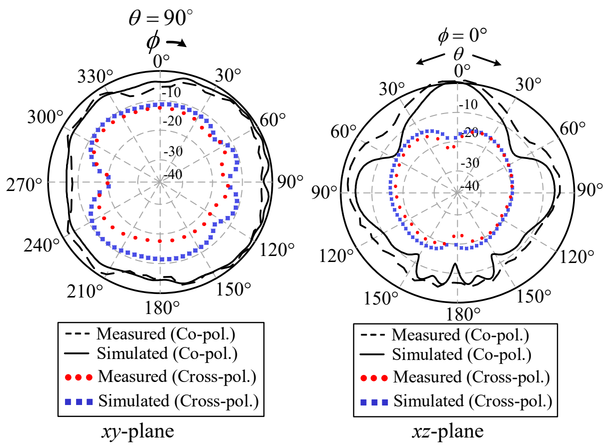

(c) at 5.00 GHz

Fig. 15. Measured radiation patterns of the split-ring coupled antenna with dipole feed in EBG at 1.42, 2.39, and 5.00 GHz in (a)–(c), respectively.

beamwidths on the *xz*-plane at 1.42, 2.39 and 5.00 GHz bands are 70, 90 and 20 degrees, respectively.

Finally, the proposed antenna is also compared to some recent works in the literature on multi-band antenna designs in [1], [2], [3] as shown in Tab. 3. It is found that the proposed antenna yields three operating frequencies with wide frequency bandwidth and high antenna gains.

Ant.	Type	Size (mm^3)	Freq. (GHz)	Gain (dBi)
[1]	Antenna array	300 × 300 × 45 in the low band and 140 × 140 × 22 in the high band	0.69–0.96 and 1.70–2.70	8.25 and 1.16
[2]	Folded patch with a vertical slot	57.7 × 117 × 29.6	0.840–0.845, 1.430–1.444, and 2.408–2.440	2.00–5.00
[3]	Asymmetrically barbed dipole antennas	62 × 62 × 40	1.131–1.312, 1.369–1.421, and 1.543–1.610	7.00–8.00 (dBic)
This work	Split-ring coupled antenna with the EBG structure	180 × 180 × 115	1.32–1.52, 2.10–2.80, and 4.90–5.20	6.00–8.00

Tab. 3. Comparison of multi-band antennas and the proposed antenna.

5. Conclusions

A split-ring coupled antenna embedded in the EBG structure is developed to produce a novel tri-band low-cost antenna with high gain radiation. The SRR and EBG structure coupling effects produce tri-band resonances, where the EBG structure additionally enhances the antenna gains. From measured results, the proposed antenna has three resonant frequencies at 1.42, 2.39 and 5.00 GHz with the uni-directional radiation patterns for wireless communications in L-band and Wi-Fi. In addition, simulation and measurement results are in good agreement for validating the design concept.

Acknowledgments

This research was funded by the King Mongkut's University of Technology North Bangkok, Contract no. KMUTNB-65-KNOW-12 and the National Science and Technology Council, Taiwan.

References

[1] JIA, F., ZHENG, Z., WANG, Q., et al. A new multi-band multi-array antenna configuration with scattering suppression for radiation pattern distortion mitigation of base station. *IEEE Transactions on Antennas and Propagation*, 2022, vol. 70, no. 7, p. 6006–6011. DOI: 10.1109/TAP.2022.3175957

[2] CUI, Y., LUO, P., GONG, Q., et al. A compact tri-band horizontally polarized omnidirectional antenna for UAV applications. *IEEE Antennas and Wireless Propagation Letters*, 2019, vol. 18, no. 4, p. 601–605. DOI: 10.1109/LAWP.2019.2897380

[3] TA, S. X., CHOO, H., PARK, I., et al. Multi-band, wide-beam, circularly polarized, crossed, asymmetrically barbed dipole antennas for GPS applications. *IEEE Transactions on Antennas and Propagation*, 2013, vol. 61, no. 11, p. 5771–5775. DOI: 10.1109/TAP.2013.2277915

[4] PAUL, P. M., KANDASAMY, K., SHARAWI, M. S. A multi-band SRR and strip loaded slot antenna. In *2018 IEEE International Symposium on Antennas and Propagation & USNC/URSI National Radio Science Meeting*. Boston (MA, USA), 2018, p. 663–664. DOI: 10.1109/APUSNCURSINRSM.2018.8608217

[5] ELAVARASI, C., SHANMUGANATHAM, T. Multiband SRR loaded Koch star fractal antenna. *Alexandria Engineering Journal*, 2018, vol. 57, no. 3, p. 1549–1555. DOI: 10.1016/j.aej.2017.04.001

[6] PENDRY, J. B., HOLDEN, A. J., ROBBINS, D. J., et al. Magnetism from conductors and enhanced nonlinear phenomena. *IEEE Transactions on Microwave Theory and Techniques*, 1999, vol. 47, no. 11, p. 2075–2084. DOI: 10.1109/22.798002

[7] NUTAN REDDY, A., RAGHAVAN, S. Split ring resonator and its evolved structures over the past decade. In *2013 IEEE International Conference on Emerging Trends in Computing, Communication and Nanotechnology (ICECCN)*. Tirunelveli (India), 2013, p. 625–629. DOI: 10.1109/ICE-CCN.2013.6528575

[8] BAENA, J. D., BONACHE, J., MARTIN, F., et al. Equivalent-circuit models for split-ring resonators and complementary split-ring resonators coupled to planar transmission lines. *IEEE*

Transactions on Microwave Theory and Techniques, 2005, vol. 53, no. 4, p. 1451–1461. DOI: 10.1109/TMTT.2005.845211

[9] KAWDUNGTA, S., JAIBANAUEM, P., PONGGA, R., et al. Superstrate-integrated switchable beam rectangular microstrip antenna for gain enhancement. *Radioengineering*, 2017, vol. 26, no. 2, p. 430–437. DOI: 10.13164/re.2017.0430

[10] NGUYEN-TRONG, N., TRAN, H. H., NGUYEN, T. K., et al. A compact wideband circular polarized fabry-perot antenna using resonance structure of thin dielectric slabs. *IEEE Access*, 2018, vol. 6, p. 56333–56339. DOI: 10.1109/ACCESS.2018.2872571

[11] KAWDUNGTA, S., TORRUNGRUENG, D., BOONPOONGA, A., CHOU, H.-T. Dual-band Huygens source antennas with partially reflective surfaces. *Radio Science*, 2022, vol. 57, no. 11, p. 1–13. DOI: 10.1029/2022RS007602

[12] TORRUNGRUENG, D., KAWDUNGTA, S., AKKARAEKTHALIN, P. An efficient analysis of the far-field radiation of an electric/magnetic Hertzian dipole embedded in electromagnetic bandgap structures of periodic lossless multilayers using the equivalent CCITL model. *Journal of Electromagnetic Waves and Applications*, 2016, vol. 30, no. 17, p. 2227–2240. DOI: 10.1080/09205071.2016.1243490

[13] WU, X. H., KISHK, A. A., GLISSON, A. W. A transmission line method to compute the far-field radiation of arbitrarily directed Hertzian dipoles in a multilayer dielectric structure: Theory and applications. *IEEE Transactions on Antennas and Propagation*, 2006, vol. 54, no. 10, p. 2731–2741. DOI: 10.1109/TAP.2006.882164

[14] DASSAULT SYSTÈMES. CST Studio Suite 2012, Dassault Systèmes, 2012, Retrieved from: https://www.3ds.com/products-services/simulia/products/cst-studio-suite/solvers/

About the Authors …

Supakit KAWDUNGTA received a Bachelor of Engineering (2006) in Telecommunications Engineering, Master of Engineering (2007) in Telecommunications Engineering, and Doctor of Engineering (2011) in Electrical Engineering from King Mongkut's Institute of Technology Ladkrabang, Bangkok, Thailand. From 2011 to the present, he is a lecturer and an Assistant Professor in Electronic and Telecommunications Engineering at Rajamangala University of Technology Lanna, Chiang Mai, Thailand.

Danai TORRUNGRUENG (corresponding author) received his B.Eng. degree in Electrical Engineering (EE) from Chulalongkorn University, Bangkok, Thailand, in 1993. He obtained his M.S. and Ph.D. degrees in EE from The Ohio State University in 1996 and 2000. From 1995 to 2000, he was a Graduate Research Assistant (GRA) in the Department of Electrical Engineering, ElectroScience Laboratory of The Ohio State University. From 2002 to 2017, he worked in the Electrical and Electronic Engineering Department in the Faculty of Engineering and Technology at Asian University, Chonburi, Thailand. At present, he is a Professor in the Department of Teacher Training in Electrical Engineering in the Faculty of Technical Education at King Mongkut's University of Technology North Bangkok, Bangkok, Thailand.

In 2000, he won an award in the National URSI Student Paper competition at the 2000 National Radio Science Meeting in Boulder, Colorado. From 2004 to 2009, he invented generalized Smith charts, called T-charts or *Meta-Smith charts*, to solve several problems associated with conjugately characteristic-impedance transmission lines (CCITLs) and bi-characteristic-impedance transmission lines (BCITLs), including their useful applications in applied electromagnetics. He authored *Meta-Smith Charts and Their Potential Applications* (Morgan & Claypool, 2010) and *Advanced Transmission-Line Modeling in Electromagnetics* (Charansanitwong Printing, 2012). His research interests are electromagnetic sensors, fast computational electromagnetics, rough surface scattering, propagation modeling, electromagnetic wave theory, microwave theory, and techniques and antennas. He is currently a senior member of the IEEE, and a member of the ECTI, where he served as an ECTI technical chair in electromagnetics from 2014 to 2017. In addition, he served as a TPC co-chair of TJMW2016, a vice co-chair of TJMW2017, and the TPC chair of ISAP2017. Furthermore, he is a *co-founder* of the Innovative Electromagnetics Academy of Thailand (iEMAT), founded in 2013.

Hsi-Tseng CHOU received his B.S. degree in Electrical Engineering from the National Taiwan University in 1988 and his M.S. and Ph.D. degrees in Electrical Engineering from The Ohio State University (OSU) in 1993 and 1996, respectively. He is currently appointed as a Distinguished Professor in the Graduate Institute of Communication Engineering and Department of Electrical Engineering, National Taiwan University, Taiwan.

Dr. Chou joined ElectroScience Laboratory (ESL) in OSU as a graduate research associate from 1991 to 1996 and a post-doctoral researcher from 1996 to 1998. His research interests include wireless communication networks, antenna design, antenna measurement, electromagnetic scattering, asymptotic high-frequency techniques such as Uniform Geometrical Theory of Diffraction (UTD), novel Gaussian Beam techniques, and UTD type solution for periodic structures.

Dr. Chou has received many awards to recognize his distinguished contributions to technological developments. Some important ones include a distinguished contribution Award in promoting inter-academic and industrial cooperation from the Ministry of Education, a distinguished engineering professor award from the Chinese Institute of Engineers, a distinguished electrical engineering professor award from the Chinese Institute of Electrical Engineering, and the University's Industrial Economics Contribution Award (2008) and National Industrial Innovation Awards—Key Technology Elite Award (2011) and Industrial-Academia Collaboration Award (2017), all from the Ministry of Economics. He was elected in 2004 as one of the nation's ten outstanding young persons by Junior Chamber International, in 2005 a National Young Person Medal from China Youth Corps of Taiwan, and as one of the top 10 rising stars in Taiwan by the Central News Agency of Taiwan. He has served as the chair of the IEEE AP-S Taipei Chapter and received the best chapter award in 2012, and is the former chair of the EMC-S Taipei chapter. He also received outstanding branch counselor awards from IEEE, including IEEE headquarter, R-10 and Taipei Section. He received the IEEE technical field undergraduate teaching award in 2014. He has published more than 493 journal and conference papers, and holds 40 patents. He is an IEEE Fellow and IET Fellow, and an elected member of URSI International Radio Science US commission B.